Hindawi
Geofluids
Volume 2020, Article ID 6644849, 12 pages
https://doi.org/10.1155/2020/6644849

Research Article

Research on Arch Model and Numerical Simulation of Critical Water and Sand Inrush in Coal Mine near Unconsolidated Layers

Guibin Zhang[1], **Wenquan Zhang**[2], **Hailong Wang**[1], **Siwen Cao**[3], **Yuliang Wu**[4] and **Zaiyong Wang**[2]

[1]*School of Civil Engineering and Architecture, Linyi University, Linyi 276000, China*
[2]*College of Energy and Mining Engineering, Shandong University of Science and Technology, Qingdao 266590, China*
[3]*Yangcun Coal Mine, Yanzhou Coal Mining Company Limited, Zhoucheng 272118, China*
[4]*Baodian Coal Mine, Yanzhou Coal Mining Company Limited, Yanzhou 273513, China*

Correspondence should be addressed to Wenquan Zhang; wenquanzhang@163.com

Received 1 November 2020; Revised 17 November 2020; Accepted 30 November 2020; Published 15 December 2020

Academic Editor: Bin Gong

With the continuous increase of the upper limit of coal mining, in mining areas near unconsolidated layers, water and sand inrush disasters occur from time to time, seriously threatening the safety of mine production. In this paper, the process of water and sand inrush accidents induced by mining near unconsolidated layers is analyzed using mechanical analysis and numerical simulation methods, based on the principle of silo unloading and arching and combined with actual water and sand inrush characteristics; the critical water and sand inrush arching mechanism is explained. The paper also proposed and established three critical arching mechanics models (interlocking arch, bonded arch, and transition arch), deduced the mathematical expression of interlocking arch and transition arch, and obtained the critical instability conditions of the arch and its influencing factors. The research results have guiding significance for the occurrence of water and sand inrush disasters and the judgment of the degree of damage in mining near unconsolidated layers.

1. Introduction

With the reduction of mine recoverable reserves, mining shallow coal seams threatened by loose aquifers has become the preferred target for mine to extend life and potential tapping innovation. However, the overlying loose aquifers are affected by mining and cause water with higher sand content. The sand mixture collapses into the underground working face, causing property losses and even death from time to time, which poses a great threat to the safety of mine production [1–4].

Since the 1990s, many Chinese scholars have conducted researches on the prediction of water and sand inrush disasters and its prevention in unconsolidated layers. Rich experience [5–9] has been obtained. Sui Wanghua et al. [10–12] proposed to use the flow behavior of particulate matter to understand the mechanism of sand break in depth and believed that the head pressure of the overlying loose aquifer and the width of the sand break channel are the key to establishing the mechanism of water and sand inrush; to increase the mining upper limit of coal seams under thick loose seams, Xu Yanchu [13, 14] studied water pressure as the key factor leading to water inrush in loose seams taking Henan Zhaogu No. 1 Coal Mine as an example and revised sand-proof coal pillar formula accordingly. LiangYankun [15] studied the propagation of chemical grout in the inclined fracture model through physical experiments, discussed that grouting can effectively reduce the critical inclination of the fracture of the water and sand mixture seepage, and concluded that the high viscosity of the cement slurry is beneficial to the sand particles. Wang Hailong and Zhang Shichuan et al. [16, 17] developed a water and sand inrush test system to study the migration and inrush laws of water and sand in the mining fractures and revealed the water and sand inrush with water pressure as a variable flow rate changes and the characteristics of water pressure changes at the bottom of the water-

bearing sand layer; Liu Qi [18] designed a stress control seepage experimental system based on particle loss and concluded that the water and sand inrush process is divided into three different stages to study the degree of consolidation of the excavated soil, and water pressure plays an important role in the seepage erosion process.

Meanwhile, some scholars have conducted comprehensive evaluation and prediction on the risk of water and sand inrush through mathematical methods [19–23]. Zhang Wenquan [24] used factor analysis (FA) and Fisher's Discriminant Analysis to establish a water and sand inrush evaluation model for aquifers under thick unconsolidated layers, concluded that the water pressure and the thickness of the bottom clay layer have a great impact on water and sand inrush, and predicted the possibility of water and sand inrush in each mine. Wang Xin [25] combined the analytic hierarchy process and entropy method to study the important effects of water inrush in the tunnel and proposed a tunnel water inrush multi-index evaluation model based on the normal cloud model based on dynamic monitoring; Peng Yaxiong [26] divided the tunnel water inrush risk into four levels, established a cloud model-based water-rich fault zone tunnel water inrush evaluation model, and verified the model through the Longjingxi tunnel. Generally speaking, the aforementioned scholars studied the key factors affecting the water and sand inrush in unconsolidated layers, but there is not much research on its internal mechanism [27, 28].

Some scholars have also conducted in-depth research on similar simulated materials. Through different ratios of similar materials, simulated materials with similar physical properties of rock formations are obtained, and the internal mechanism of thick loose seams in the process of coal mining is analyzed through internal physical experiments, the law of sinking [29–32].

In summary, the research on water and sand inrush disasters has achieved staged results. However, with the continuous lifting of the coal mining limit, the number and distribution of mining wells involved have gradually expanded, and the hydrogeological and engineering geological conditions of the mines have also become complex and changeable. Therefore, to clarify the key factors that induce water and sand inrush and the mechanism of each key factor on water and sand inrush is an effective method to analyze its mechanism. Based on the arching mechanism of silo discharge, this paper puts forward the hypothesis of critical water and sand inrush arching, classifies the critical arching types of water and sand inrush, and analyzes the characteristics and instability of critical arches of various water and sand inrushes. The judgment criterion, combined with the mathematical model to study the instability judgment law, has guiding significance for the occurrence of water and sand inrush disasters and the damage degree judgment in mining of near unconsolidated layers.

2. Mechanical Model and Off-Stability Conditions of Water and Sand Inrush

By comparing the arching mechanism of silo discharge with unconsolidated layer's characteristics of sand particle distribution and clay composition, the paper proposes a critical water-sand inrush arching model and analyzed the structural characteristics of the critical arch of water-sand and destruction instability mechanism.

Similar to the principle of silo unloading and arch formation, when mining near unconsolidated layers and the overlying strata penetrate the aquifer, water inrush (gush) or water and sand inrush will occur. The difference between water inrush (gush) and water and sand inrush is whether solid sand particles can migrate on a large scale under the driving force. On the other hand, water inrush (gush) without sand ingress means after the mining crack and unconsolidated layer aquifer penetrate, the water and sand will continue to converge towards the fracture of the crack and gush out along the channel under the drive of the power source. However, due to the limited space of the crack channel, the sand will squeeze with each other and form a stable structure somewhere near the fracture channel, which prevents the upper sand body from moving until it stops, and water will gush out through the pores between the sand bodies. Once the steady sand body structure being destroyed, instability occurs, or the channel is wide enough that unable to form such a stable structure; it will induce water and sand inrush. The author believes that the steady-state structure of sand is distributed in an "arch" shape and proposes the critical water and sand inrush arch theory, summarized as the critical interlocking arch of water-sand inrush, the critical bonding arch of water and sand inrush, and the critical transitional arch of water-sand inrush. The specific features of each arch are as follows:

(1) The critical interlocking arch of water and sand inrush is due to the compression between sand particles and rock wall, and between particles near the opening of the mining fracture channel, resulting in the interlocking of the contact forces between the contact points to form an "arch" force chain, when it can bear the upper load and the force is balanced, arch is therefore formed. This kind of arch is more often seen in aquifer of unconsolidated layers with sand, coarse sand, medium sand, silt fine sand, and other sand with relatively large particle size and less viscous components

(2) Critical bonding arches of water and sand inrush are mostly formed in silty or clay soil layers (for example, clay layers and silty clay layers) that contain a lot of viscous components with relatively good bonding properties and small and uniform particle size. The arch is mainly stabilized by the adhesion between particles and internal friction

(3) Due to the complex depositional environment of loose strata, the grain size and viscous components of sand are generally diverse. Therefore, the paper proposed the critical transition arch for water and sand inrush, which has the characteristics of interlocking arch and bonded arch, that is to say, arch's body structure is formed by the joint force of the squeezing interlocking force chain and the cohesive

force between clay particles. It occurs in sand layers with various particle sizes with a certain clay composition, such as clayey gravel and coarse clay sand

2.1. Interlocking Arch Mechanics Model and Off-Stability Conditions. According to the simplification of loose granular materials in granular structural mechanics [33], the sand quality of interlocking arch can be regarded as ideal granular; since the formation of interlocking arch is mainly caused by the interaction between particles and other factors, discrete medium model (discrete discontinuous medium as a calculation model) should be selected to reveal the law of interaction between particles, so as to analyze the formation of interlocking arch and its instability mechanism reasonably.

The particle arches are divided into two types, considering the arching of sand particles: odd-numbered and even-numbered arrangements. Respective mechanical models are established as shown in Figures 1 and 2.

The mechanical model of the particles arranged in odd number on the arch is shown in Figure 1(a). The unit width of the left half arch is selected as the calculation model. The force of the left half arch at current situation: the force T_1 of the right half arch on the left half arch and the horizontal angle is θ while the friction between the two is the force F_f. The left half arch is subjected to the external pressure F_N in the horizontal direction and is subjected to the vertical downward compressive stress F of the overlying strata and the seepage pressure F_s of water (it can be characterized by the sum of the drag force F_D and the viscous force F_u). The floating weight from the side half arch itself is W and the supporting force T_2 (the angle with the horizontal direction is α) and the friction force F_{f2} of the rock wall to the left half arch.

When the model reaches critical equilibrium, the mechanical equilibrium conditions of the left half arch in the vertical and horizontal directions are as follows:

Mechanical equilibrium conditions of the left half arch in the vertical direction:

$$F_D + F_u + W + F = T_1 \sin\theta + T_2 \sin\theta + F_f + F_{f2}. \quad (1)$$

Namely,

$$(\sigma_D + \sigma_u + \sigma_1 + \sigma)\frac{D}{2} = T_1 \sin\theta + T_2 \sin\alpha + \tan\phi_1 T_1 \cos\theta + \tan\phi_2 T_2 \cos\alpha = \frac{\sigma' D}{2}. \quad (2)$$

In the formula, φ_1 is the internal friction angle between sand particles, °; φ_2 is the internal friction angle between the rock wall and the sand, °; α is the angle between the rock wall supporting force T_2 of the left half arch and the horizontal direction, °; θ is the pressure angle of the arch line at the arch crown, °; σ' is the total vertical downward stress on the left half arch, that is the sum of σ_D, σ_u, σ_1, and σ.

The horizontal mechanical equilibrium of the left half arch:

$$F_N + T_2 \cos\alpha = T_1 \cos\theta. \quad (3)$$

Among them, the external lateral stress $F = \sigma' kh$,

$$\sigma' kh + T_2 \cos\alpha = T_1 \cos\theta. \quad (4)$$

In the formula, h is the height of the arch while k is the pressure measurement coefficient, $k = (1\text{-}\sin\phi_1)/(1 + \sin\phi_1)$, and φ_1 is the internal friction angle of sand particles [33].

Take the moment O point of the left half arch, $\sum M_0 = 0$: $(F'D/4) + (F_N h/2) = T_1 \cos\theta h + T_1 \sin\theta(D/2) + T_1 \cos\theta \cdot \tan\phi_1 \cdot (D/2)$, namely, $(\sigma' D^2/8) + (k\sigma' h^2/2) = T_1 \cos\theta \cdot h + T_1 \sin\theta \cdot (D/2) + T_1 \cos\theta \cdot \tan\phi_1 \cdot (D/2)$, transferred to

$$T_1 = \frac{\sigma'\left(\left(D^2/8\right) + \left(kh^2/2\right)\right)}{\cos\theta \cdot h + \sin\theta \cdot (D/2) + \cos\theta \cdot \tan\phi_1 \cdot (D/2)}. \quad (5)$$

In the formula, F' is the left half arch subjected to a vertical downward force.

As shown in Figure 1(b), this is the force analysis of a single particle in the dome, and the vertical force equilibrium condition:

$$\sigma' d = 2T_1 \sin\theta + 2T_1 \cos\theta \cdot \tan\phi_1. \quad (6)$$

After transformation,

$$T_1 = \sigma' \frac{d}{2}(\sin\theta + \cos\theta \cdot \tan\phi_1). \quad (7)$$

Combining and simplifying formula (5) and formula (7), we can get

$$\frac{d}{\left(D^2/8\right) + \left(kh^2/2\right)} = \frac{4(\tan\theta + \tan\phi_1)}{D(\tan\theta + \tan\phi_1) + 2h}. \quad (8)$$

Brador Yakonov's theory believes the relationship between the dynamic falling arch height h and the critical orifice outflow diameter D and the internal friction coefficient f of the material [34]:

$$h = \frac{D}{2f}. \quad (9)$$

In the formula, f is the internal friction coefficient between sand particles, namely $f = \tan\varphi_1$.

From the combination and simplification of formula (8) and formula (9), the formula for the maximum crack width of the critical instability of the interlocking arch with odd-numbered arrangement of sand particles can be expressed as:

$$D = \frac{2d}{1 + \left(k/f^2\right)}\left(1 + \frac{1}{\tan\theta \cdot f + f^2}\right). \quad (10)$$

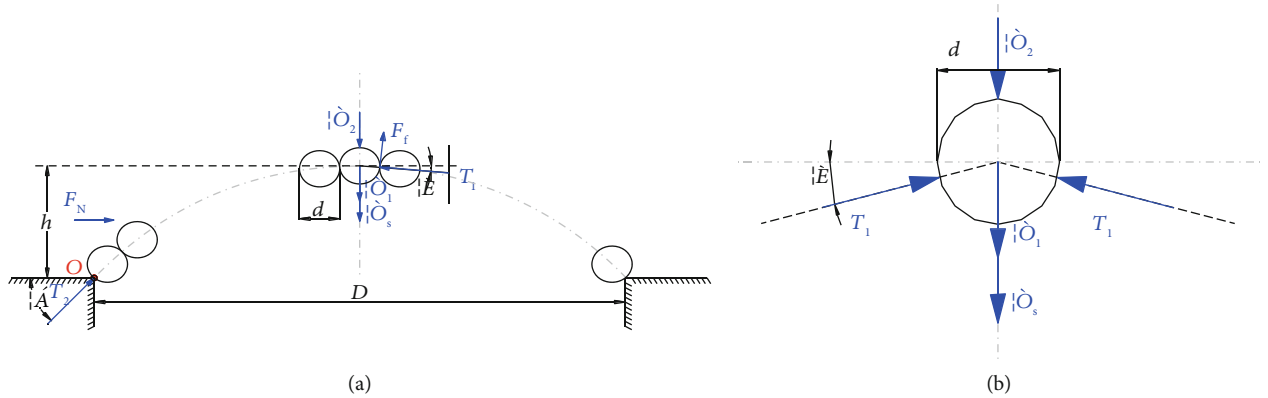

Figure 1: Mechanical model of odd number of sand particles.

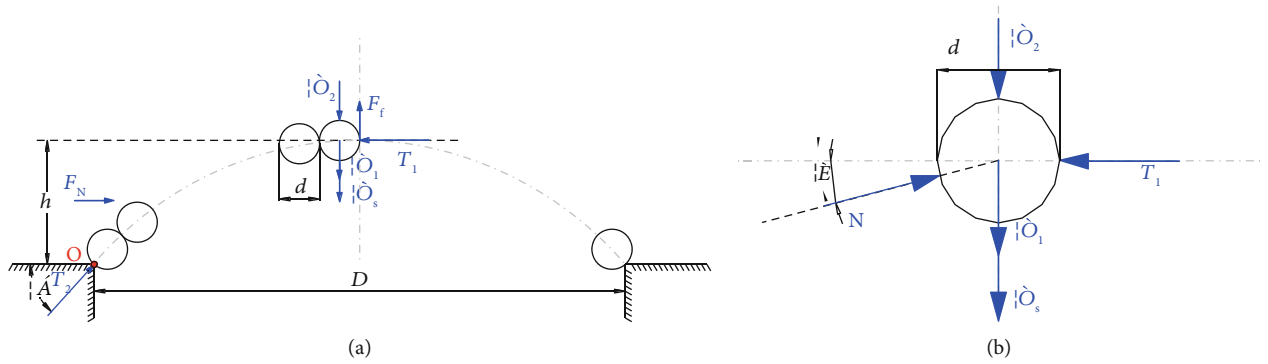

Figure 2: Mechanical model of even number of sand particles.

In the formula, f is the internal friction coefficient between sand particles, namely, $f = \tan \varphi_1$; k is the pressure measurement coefficient, $k = (1\text{-}\sin \phi_1)/(1 + \sin \phi_1)$; $\varphi 1$ are the internal friction angle of the sand particles; θ is the pressure angle of the arch line at the arch crown; d is the diameter of the sand particles.

It can be seen from formula (10) that the larger the sand body particle is, the larger the maximum crack width required for the arch instability of the particle will be; it can be seen from the transformation the critical ratio of crack width to sand particle size (it is referred to as the ratio of crack and sand), namely,

$$i_{\max} = \frac{D}{d} = \frac{2}{1 + \left(k/f^2\right)}\left(1 + \frac{1}{\tan\theta \cdot f + f^2}\right). \tag{11}$$

From the analysis of formula (11), it can be seen that when the sand body is a nearly ideal granule with less viscosity and relatively large particle size; when its ratio of crack and sand i is less than or equal to $i_{\max}$, an arch will be formed at the crack opening that hinders the upper body movement, resulting in no water and sand inrush. Otherwise, it will cause water and sand inrush disaster.

The mechanical model of the particles arranged in an even number array of the arch, and force conditions are shown in Figure 2(a). The unit width of the left half arch is selected for analysis. When the model reaches critical equilibrium, the mechanical equilibrium conditions of the left half arch in the vertical and horizontal directions are as follows:

Mechanical equilibrium equation of the left half arch in the vertical direction:

$$F_D + F_N + W + F = T_2 \sin\alpha + F_f + F_{f2}. \tag{12}$$

Namely,

$$\begin{aligned}(\sigma_D + \sigma_u + \sigma_1 + \sigma) \cdot \frac{D}{2} &= T_2 \sin\alpha + T_1 \tan\phi_1 + T_2 \cos\alpha \cdot \tan\phi_2 \\ &= \frac{\sigma' D}{2}.\end{aligned} \tag{13}$$

In the formula, φ_1 is the internal friction angle between sand particles, °; φ_2 is the internal friction angle between the rock wall and the sand, °; α is the angle between the rock wall supporting force T_2 of the left half arch and the horizontal direction, °; θ is the pressure angle of the arch line at the arch crown, °; σ' is the total vertical downward stress on the left half arch, that is the sum of σ_D, σ_u, σ_l, and σ.

The horizontal mechanical equilibrium of the left half arch:

$$F_N + T_2 \cos\alpha = \sigma' kh + T_2 \cos\alpha = T_2 \cos\theta. \quad (14)$$

In the formula, F_N is the external lateral stress $F_N = \sigma' kh$, F' is the resultant vertical downward force on the left half arch; h is the arch height; k is the lateral pressure coefficient; $k = (1\text{-}\sin\phi_1)/(1 + \sin\phi_1)$; φ_1 is the internal friction angle of sand particles.

Take the moment O point of the left half arch, $\sum M_0 = 0$: $(F'D/4) + (F_N h/2) = T_1 h + T_1 \tan\phi_1 (D/2)$, namely, $(\sigma' D^2/8) + (k\sigma' h^2/2) = T_1 h + T_1 \tan\phi_1 \cdot (D/2)$, transformed into

$$T_1 = \frac{\sigma'\left(\left(D^2/8\right) + \left(kh^2/2\right)\right)}{h + \tan\phi_1 \cdot (D/2)}. \quad (15)$$

As shown in Figure 2(b), the force analysis of a single particle in the arch:

$$\text{Vertical force equilibrium condition}: \sigma' d = T_1 \tan\phi_1 + N\cos\theta \tan\phi_1 + N\sin\theta. \quad (16)$$

$$\text{Horizontal force equilibrium condition}: N\cos\theta = T_1. \quad (17)$$

In could be conducted from formula (16) and formula (17) that

$$T_1 = \frac{\sigma' d}{2\tan\phi_1 + \tan\theta}. \quad (18)$$

Combining formula (15) and formula (18) with Brador Yakonov's theory, after simplification, we could get the formula for the maximum crack width of the critical instability of the even-numbered arrangement of sand particles:

$$D = \frac{4d\left(f + f^3\right)}{(2f + \tan\theta)\left(f^2 + k\right)}. \quad (19)$$

In the formula, f is the internal friction coefficient between sand particles, namely, $f = \tan\varphi_1$; k is the pressure measurement coefficient, $k = (1\text{-}\sin\phi_1)/(1 + \sin\phi_1)$; φ_1 is the internal friction angle of the sand particles; θ is the characterize the pressure angle of the arch line at the arch crown; d is the diameter of the sand particles.

By transforming formula (19), the critical cracking particle ratio of the even-numbered arrangement of sand body interlocking arch instability can be conducted:

$$i_{\max} = \frac{D}{d} = \frac{4\left(f + f^3\right)}{(2f + \tan\theta)\left(f^2 + k\right)}. \quad (20)$$

From the analysis of the above formulas (9), (10), (19), and (20):

(1) Whether particles are arranged in odd or even numbers, its critical instability maximum crack width of the interlocking arches formed goes up with the increase of sand particles with proportional relationship; it is also clear that the crack width is constant under certain conditions, the larger the particle size of the sand body, the easier the arch to form. On the contrary, the arch instability will cause water and sand inrush

(2) For nearly ideal granular particles, the critical cracking ratio of the interlocking arch is mainly subject to its own properties (internal friction angle). At the same time, the pressure angle θ at the arch crown also has a certain influence on it. The mechanical environment (such as vertical compressive stress, and lateral stress) has little influence, that is to say, the change of external force basically does not affect the critical ratio of crack or instability conditions of the nearly ideal granular interlocking arch

2.2. Transition Arch Mechanics Model and Off-Stability Conditions. The water-sand inrush bonded arch is mainly caused by cohesive force and internal friction between particles to maintain the stability of the arch structure. It is mostly formed in the silty or clay soil layer with good cohesiveness. The calculation model of viscous granular medium is often used in granular structural mechanics, which is mainly applied in overall research, such as overall flow and shear failure. However, in actual conditions, such conditions represent the presence of a clay layer at the bottom of the unconsolidated layers. Generally, it is difficult to induce water and sand inrush when the overburden mining damage degree and the crack width are small; therefore, no major research was conducted in this regard.

As for the sandy aquifer at the bottom of the unconsolidated layers with a certain amount of clay, its own sand quality is between the ideal granule and the cohesive granule. Based on the foregoing analysis, critical water and sand inrush transitioning arch is proposed for this type of sand. From the analysis of the overall sand body characteristics, it is similar with the cohesive granules since the clay sand possesses certain cohesive force: they are all granules with certain tensile capacity, shear resistance, and internal friction but with difference in mechanical parameters. Therefore, based on the calculation model of the viscous granular medium, this paper establishes a mechanical model of the critical transition arch for water and sand inrush and analyzes the judging conditions of off-stability model.

According to the characteristics of the transition arch sand body and the arching mechanism analysis, it is believed that when the overlying strata penetrates the sandy aquifer at the bottom of the unconsolidated layers, water will flow into the working face along the crack channel, and the water level above the crack will begin to drop, ending up with a difference in water head between the initial water levels in distant aquifer and caused hydrodynamic pressure. Therefore, the sand body above the fracture is subject to hydrostatic pressure (buoyancy), its own gravity W, the positive pressure F

of the upper formation, the lateral pressure F_N of the formation, frictional force F_f between sand bodies, and the cohesive force. In addition to aforementioned forces, it is also subject to hydrodynamic pressure, namely, seepage pressure F_s; when the vertical downward total stress σ' of the sand body in the upper arch of the fracture opening exceeds the ultimate shear strength τ_{max}, the sand body starts to migrate, resulting in the instability of the arch and water and sand inrush. This is the mechanical condition for the critical instability of the transitional arch, namely,

$$\sigma' \geq \tau_{max}, \tag{21}$$

where $\tau_{max} = \sigma \tan \phi + c$ [35], σ is the lateral stress; φ is the internal friction angle; c is the cohesion of sand.

On-site mining fracture channels are mainly fracture, and the infinitely long fracture type water-sand inrush transitional arch critical instability mechanical model is established, as shown in Figure 3. It can be regarded as a plane strain issue, and the unit thickness in the vertical direction is taken as the research object, and the critical instability conditions of the water-sand inrush transition arch are analyzed as follows.

Assuming that the thickness of the aquifer is M, the overlying is a stable aquifer (without vertical hydraulic recharge), and the initial water head height of the aquifer at infinity is h, and the permeability coefficient of the aquifer is K, with porosity being n. When the overlying strata and the aquifer are connected, the width of the crack is D, which just reaches the critical instability mechanical equilibrium state of the transition arch. The aquifer at the upper part of the crack is divided into several columns of unit width by the method of striping. At this time, each sand column or sandy unit above the fracture could be expressed in formula (21); considering that the critical crack width is relatively small, after penetrating the aquifer, a hydraulic gradient funnel with the fracture centerline as the symmetry axis is formed, and the height of the water head above the fracture is approximately equal to that of the horizontal aquifer (the water head equipotential line is approximately horizontal), so it can be approximated that the sandy unit above the fracture is subjected to vertical downward seepage pressure F_s, so the upper part of the fracture in the sandy unit abcd at the bottom of the central unit width column is selected as the research object. As can be seen from Figure 3, the water head height at this time is h_1, and the top and bottom interface water heads of the sandy unit abcd at the bottom of the column are ha(b) and hc(d), respectively, with the height difference between the two is $\triangle h$.

After the force analysis of the sandy unit abcd, mechanical equilibrium conditions of critical instability could be expressed as

$$F_s + W' = 2F_f + C_E. \tag{22}$$

In the formula, F_s is the seepage pressure of the sandy unit; W' is the floating weight of the sandy unit; F_f is the frictional resistance of the sandy unit; C_E is the cohesion of the sandy unit.

$$\text{Floating weight of sandy unit in water}: W' = (1-n)(G_s - 1)\gamma_w. \tag{23}$$

$$F_s \text{ is the seepage pressure of the sandy unit}: F_s = \gamma_w J = \gamma_w \Delta h. \tag{24}$$

$$F_N \text{is the lateral pressure}: F_N = \xi \gamma' H. \tag{25}$$

$$F_f \text{ is the frictional resistance of the sandy unit}: F_f = F_N \tan \phi = \xi \gamma' H \tan \phi. \tag{26}$$

$$C_E \text{is the cohesion of the sandy unit}: C_E = f(n, a, C). \tag{27}$$

In the formula, G_s is the relative density of sand particles; n is the porosity of sand; r_w is the gravity of water; J is the hydraulic gradient; $\triangle h$ is the water head height difference between top and bottom interface of sandy unit; ζ is the lateral pressure coefficient; H is the depth of sandy unit; γ' is the average density of unconsolidated layers above sandy unit.

Based on the above analysis, the author introduced confirmed various forces into formula (22) to obtain the equilibrium conditions for the critical instability of the transition arch:

$$(1-n)(G_s - 1)\gamma_w + \gamma_w \Delta h = 2\xi \gamma' H \tan \phi + C_E. \tag{28}$$

The critical hydraulic gradient J' of the sandy unit body could be expressed after simplification:

$$J' = \Delta h = \frac{\left(2\xi \gamma' H \tan \phi + C_E\right)}{\gamma_w} - (1-n)(G_s - 1). \tag{29}$$

According to Darcy's law, the seepage velocity form is

$$v = KJ. \tag{30}$$

In the formula, v is water seepage velocity; J is hydraulic slope; K is permeability coefficient.

Combining formulas (28) and (29), the critical water flow velocity v_{cr} of the transition arch instability can be expressed as

$$v_{cr} \geq K\left(\frac{2\xi \gamma' H \tan \phi + C_E}{\gamma_w} - (1-n)(G_s - 1)\right). \tag{31}$$

According to formula (31), it can be seen that when the groundwater seepage velocity at the crack opening is greater than v_{cr}, water and sand inrush will occur, and with the increase of internal friction angle, cohesive force, and aquifer buried depth, the higher the critical water flow velocity is required for off-stability of arch. It can also be explained that the stability of the transition arch formed by the sand with a certain cohesion is affected by the characteristics of the sand and the external mechanical environment.

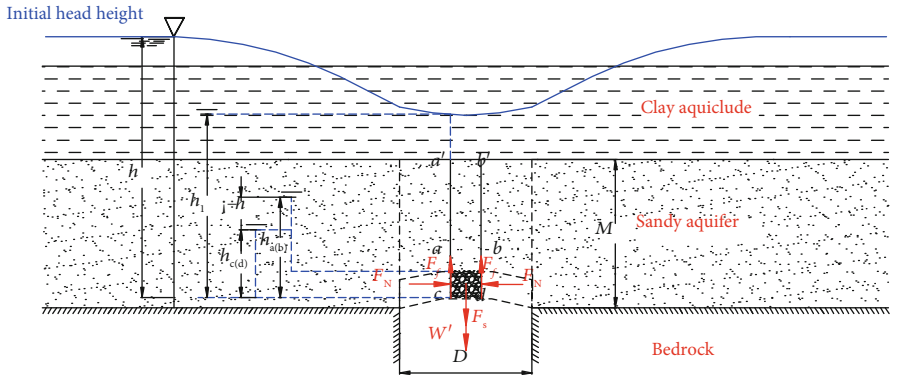

Figure 3: Mechanical model of critical instability of water and sand inrush transition arch.

Table 1: Main conditions and parameters of simulation.

Size of the cabin (m)	Particle size d (m)	Particle normal bond strength (N)	Tangential bond strength (N)	Initial porosity rate	Particle normal stiffness (N·m^{-1})	Particle tangential stiffness (N·m^{-1})
0.6 × 0.4	0.01 m	0	0	0.15	10^9	10^9

As for determining groundwater seepage velocity, the formed fracture channel could be compared to a single-well steady flow pumping of a complete well with an equivalent radius [36], and different types of large wells water inflow prediction formula could be selected according to the actual aquifer characteristics and water level to estimate the amount of inflow; then, the actual seepage velocity of the groundwater can be approximated according to the principle of equivalent area of the fracture, and the critical seepage velocity can be compared to determine whether water and sand inrush will occur.

3. Numerical Simulation of Arching Mechanism of Critical Water and Sand Inrush

In this section, the discrete element numerical simulation software PFC2D is used to establish a silo-type water and sand inrush model. By changing the simulation factors (such as crack width, water pressure, and cohesive force), the critical arch loss of different types of water and sand inrush and characteristics of stability and its main influencing factors are discussed to verify the correctness of the aforementioned critical water-sand inrush arching mechanism.

3.1. Mesoanalysis of Interlocking Arches with Water and Sand Inrush. In order to analyze the critical conditions for the instability of the water and sand inrush interlocking arch and its influencing factors, a cabin model with the size of 0.6 m × 0.4 m is established. The sand body is a noncohesive uniform particle with a particle size d of 0.01 m. By changing the single variable, the author studied the effects of cracked particle ratio, water pressure, and internal friction coefficient's influence on the critical conditions of interlocking arch instability. The main conditions and parameters of the specific simulation are shown in Table 1.

3.1.1. The Critical Ratio of Crack of Interlocking Arch Instability. To obtain the critical ratio of crack of interlocking arch instability under certain conditions, the author first sets the water pressure and internal friction coefficient at 2 MPa and 0.58 (i.e., 30° friction angle), then simulates one by one by continuously adjusting the crack width, and finally, obtains the critical ratio of crack of arch instability under the condition. The specific simulation situation is shown in Figure 4. In Figures 4(c), 5, 6, and 7, the black line represents the force chain, and the blue line represents the velocity vector of water seepage.

It can be clearly seen from Figures 4 and 5 that under the ratio of crack and sand of 4.7 and 4.8, particles squeeze and arch at the crack openings, and a stable arch force chain is formed, which leads to the termination of sand collapse; when the ratio is 4.9, there is no arching. Therefore, we could reach the conclusion that under current situation, the critical crack ratio of interlocking arch is 4.9, and with the increase of crack ratio, the slope angle of the sand body gradually decreases.

3.1.2. The Influence of Hydraulic Pressure on the Critical Ratio of Crack and Sand of Interlocking Arch Instability. In order to further analyze the influence of hydraulic pressure on the critical ratio of crack and sand of interlocking arch instability, the water pressure was changed to 0.001 MPa and 1 MPa, respectively, based on the above simulation results. After the comparison on the criticality of interlocking arch instability under various water pressure conditions, the specific simulation results of the variation of the ratio of crack and sand are shown in Figure 6.

It can be seen from Figure 6 that when the ratio of crack and sand is 4.9, the cracks are arched where the hydraulic pressure is 0.001 MPa and 1 MPa with obvious accumulation of sand bodies when the water pressure is low, but the amount of sand inflow between the two is almost the same; when the ratio of crack and sand is 5.0, the arch instability

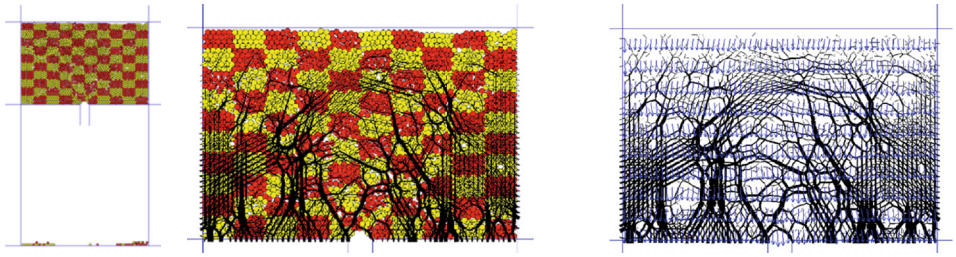

(a) Model (b) Partial zooming in (c) Force chain and velocity vector of water seepage

Figure 4: Simulation results of interlocking arch forming (supposing ration of crack and sand i being 4.7).

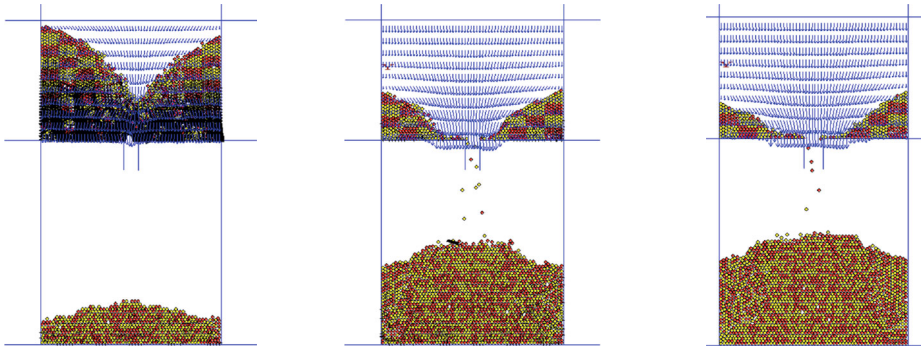

(a) Ratio of crack and sand being 4.8 (b) Ratio of crack and sand being 4.9 (c) Ratio of crack and sand being 6.0

Figure 5: Simulation results of critical instability of interlocking arch.

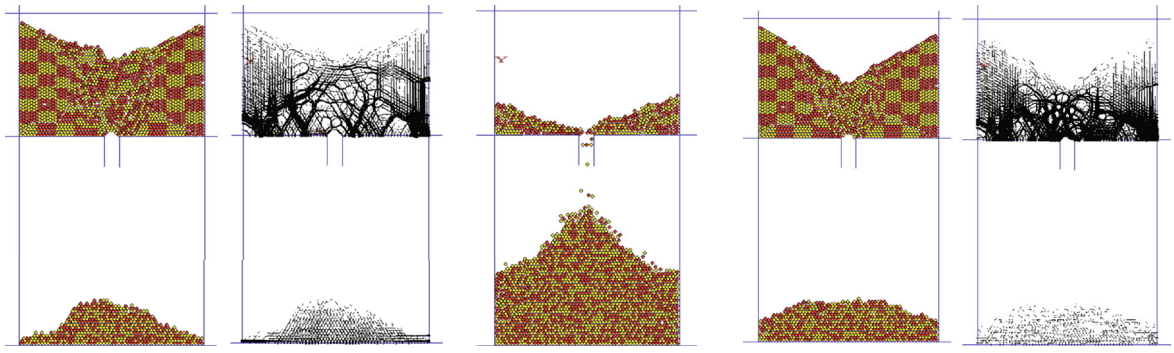

Ratio of crack and sand being 4.9 Ratio of crack and sand being 5.0 Ratio of crack and sand being 4.9

(a) Hydraulic pressure 0.001 MPa (b) Hydraulic pressure 1 MPa

Figure 6: Simulation results of critical instability of interlocking arch under different hydraulic pressure.

occurs; it can be concluded that the critical ratio of crack and sand of the arch instability is 5.0 when the hydraulic pressure is 0.001 MPa and 1 MPa, which only increases by 0.1 compared with that when hydraulic pressure of 2 MPa. It is safe to say that hydraulic pressure basically brings no effect to the critical ratio of crack and sand of the ideal unconsolidated layers interlocking arch instability. This conclusion is consistent with the aforementioned conclusion of the critical instability criterion of the arch.

3.1.3. The Effect of Internal Friction Coefficient on the Critical Crack Ratio of Interlocking Arch Instability. In order to further analyze the influence of the internal friction coefficient of the particles on the critical fracture ratio of the interlocking arch instability, the author divided the internal friction coefficient into four levels: 0.1, 0.3, 0.58, and 1, with hydraulic pressure being 2 MPa. By stimulating critical cracking ratio of interlocking arch instability under the condition of internal friction coefficient, the followed specific simulation results are reached and shown in Table 2.

It can be seen from Figure 8 that with the increase of the friction coefficient within the particles, the critical ratio of crack and sand of the arch instability increases significantly. The functional relationship between the two is obtained by fitting regression:

$$i_{\max} = -1.59083e^{(-(f/0.2246))} + 5.0912 (\text{degree of fitting R2} = 0.9999). \tag{32}$$

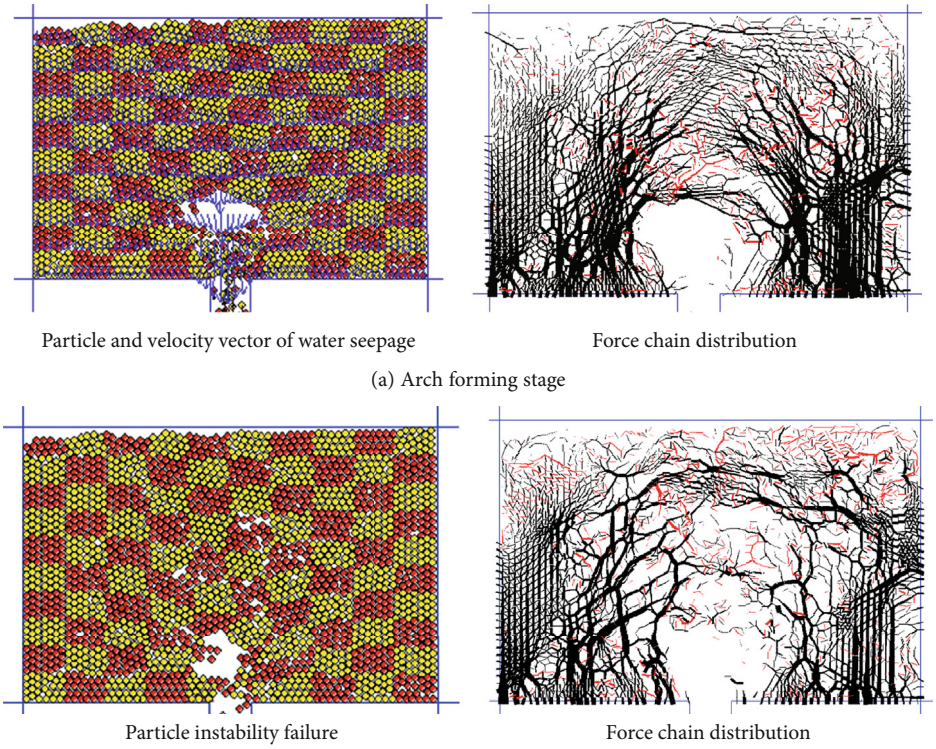

Figure 7: The transition arch destruction process simulation.

Table 2: Simulation results of ratio of crack width to particle diameter when the interlocking arch of different internal friction coefficient of granular buckling.

Internal friction coefficient f	0.1	0.3	0.58	1
Internal friction angle φ	5.7°	16.7°	30°	45°
Ratio of crack and sand i_{max}	4.0	4.6	4.9	5.0

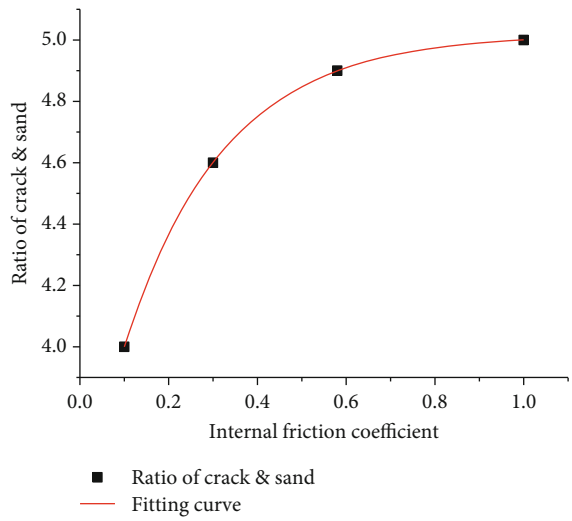

Figure 8: Relationship between the internal friction coefficient and the ratio of crack width to particle (crack and sand) diameter when interlocking arch buckling.

In the formula, f is the internal friction coefficient of the sand body; i_{max} is the critical crack and sand ratio of the interlocking arch instability.

It can be seen that for noncohesive sand bodies, the internal friction angle or the internal friction coefficient plays a decisive role in the critical fracture ratio of interlocking arches, and the critical fracture ratio gradually goes up with the increase of the internal friction coefficient. This conclusion is consistent with the aforementioned conclusion of the critical instability criterion of the arch.

At the same time, according to the analysis, the internal friction angle of the sand body goes up with the increase of the buried depth and is generally less than 30°, and when the buried depth is less than 300 m, the internal friction angle increases significantly. It can be concluded that the ratio of crack and sand for water and sand increases when the buried depth of sand bodies with same properties increases, that is, shallow-buried sand bodies are more prone to water-sand inrushes than deeper-buried sand bodies.

3.2. Mesoanalysis of Transition Arch for Water and Sand Burst. The main difference between transitional arch and interlocking arch is the cohesive force between sand particles. In this section, the simulation studies the effects of cracked particle ratio, hydraulic pressure, and particle bond strength on the critical conditions of transition arch instability. The main conditions and parameters of the specific simulation are shown in Table 3.

Table 3: Main conditions and parameters of simulation.

Size of the cabin (m)	Particle size d (m)	Coefficient of internal friction f	Initial porosity rate	Particle normal stiffness ($N \cdot m^{-1}$)	Particle tangential stiffness ($N \cdot m^{-1}$)
0.6×0.4	0.01 m	0.58	0.15	10^9	10^9

Table 4: Simulation results of ratio of crack width to particle diameter when the transition archs buckling under different conditions.

Hydraulic pressure (MPa)	2.0	2.0	2.0	2.0	2.0	0.001	0.001	0.001
Particle's bonding strength (N)	$1.5e^6$	$1e^6$	$5e^5$	$1e^5$	$1e^3$	1	$1e^3$	$1e^4$
Critical ration of crack and sand i_{max}	15.0	8.6	5.9	5.0	4.9	4.9	5.2	5.4

3.2.1. The Arch Form and Failure Instable Characteristics of Grain Transition Arch. Taking the situation where hydraulic pressure of 2 MPa and the particle bond strength of 1.0×10^6 N as an example, the critical fracture ratio of arch instability under this condition is 8.6 through multiple simulations. The specific simulation results are shown in Figure 7.

It can be seen from Figure 7 that compared with interlocking arches, the arch space formed by transition arches is relatively large, and the stability of the arch structure is maintained by the squeezing interlocking force chain and the cohesive force chain between the particles. When the external force exceeds the ultimate strength of the arch, the force chain between the particles breaks, resulting in instability and failure of the arch (Figure 7(b)); it can be seen from the figure that when the arch is destructed, the stable structure of itself and the upper sand body is broken and begins to migrate to the entrance of the channel. Since the adhesive property between particles has been destroyed, the probability of reforming an arch is extremely low. Therefore, once the transition arch becomes unstable, water and sand inrush will happen.

3.2.2. Influencing Factors of Critical Instability Failure of Transition Arch. The hydraulic pressure and particle's bonding strength were changed to obtain the critical cracking ratio of arch instability under different conditions. The specific results are shown in Table 4.

From the results in Table 4, it can be seen that the critical ratio of crack and sand of transition arch instability is affected by both the hydraulic pressure and the particle bond strength; in general, the critical ratio of crack and sand decreases with the increase of hydraulic pressure and increases with the bond strength's rising.

4. Conclusion

(1) Combining the principle of silo discharge arching, the paper proposed mechanism of critical water-sand inrush arching is proposed and determined three critical water and sand inrush arching types: interlocking arches, bonded arches, and transition arches with characteristics and applicable conditions, respectively

(2) The discrete medium mechanics model was selected for noncohesive sand bodies. The mechanics models of interlocking arches with odd and even arrangements of sand particles were established, respectively, and the ratio of critical crack width to particle size i_{max} for arch instability was obtained. In general, the critical ratio is related to the internal friction angle of the sand body itself and is slightly affected by the mechanical environment

(3) The calculation model of the viscous granular medium is selected for the viscous sand body. The mechanical model of the sand body transition arch is established, and the critical water flow velocity v_{cr} of the transition arch instability is obtained. The stability of the transition arch is related to the sand body itself. The characteristics are related to the external mechanical environment

(4) The critical crack ratio of interlocking arch instability is mainly affected by the internal friction angle between particles or the internal friction coefficient. The inner friction coefficient of shallow buried sand is smaller than the deeper ones', and the required critical crack ratio is small; therefore, water and sand inrush are more likely to occur. The critical instability of the transition arch is affected by the bond strength of the sand body and the external mechanical environment of the arch at the same time, which is consistent with the analysis conclusion of the instability condition of the arch mechanical model

Data Availability

The data used to support the findings of this study are included within the article.

Conflicts of Interest

The authors declare no conflicts of interest.

Acknowledgments

This work was supported by the National Natural Science Foundation of China (51774199 and 51704152) and the Natural Science Foundation of Shandong Province (ZR2017BEE001).

References

[1] X. Yang, Y. Liu, M. Xue, T. H. Yang, and B. Yang, "Experimental investigation of water-sand mixed fluid initiation and migration in porous skeleton during water and sand inrush," *Geofluids*, vol. 2020, Article ID 8679861, 18 pages, 2020.

[2] H. Li, J. Li, L. Li, H. Xu, and J. Wei, "Prevention of water and sand inrush during mining of extremely thick coal seams under unconsolidated Cenozoic alluvium," *Bulletin of Engineering Geology and the Environment*, vol. 79, no. 6, pp. 3271–3283, 2020.

[3] Z. Ahmad, U. K. Singh, and A. Kumar, "Incipient motion for gravel particles in clay-silt-gravel cohesive mixtures," *Journal of Soils and Sediments*, vol. 18, no. 10, pp. 3082–3093, 2018.

[4] J. Israr and B. Indraratna, "Study of critical hydraulic gradients for seepage-induced failures in granular soils," *Journal of Geotechnical and Geoenvironmental Engineering*, vol. 145, no. 7, 2019.

[5] N. C. D. Santos, L. M. M. S. Caldeira, and E. M. D. Neves, "Experimental study on crack filling by upstream fills in dams," *Geotechnique*, vol. 65, no. 3, pp. 218–230, 2015.

[6] A. Ghirlan and M. Fall, "Coupled thermo-hydro-mechanical-chemical behaviour of cemented paste backfill in column experiments," *Engineering Geology*, vol. 170, pp. 11–23, 2014.

[7] B. B. Yang, *Spatio-Temporal Variation of Fractures in Overburden Due to Mining and Risk Assessment Model for Water and Sand Inrush*, China University of mining and technology, China, 2018.

[8] G. Zhang, K. Zhang, L. Wang, and Y. Wu, "Mechanism of water inrush and quicksand movement induced by a borehole and measures for prevention and remediation," *Bulletin of Engineering Geology and the Environment*, vol. 74, no. 4, pp. 1395–1405, 2015.

[9] Z.-w. Qian, Z.-q. Jiang, Y.-z. Guan, and N. Yue, "Mechanism and remediation of water and sand inrush induced in an inclined shaft by large-tonnage vehicles," *Mine Water and the Environment*, vol. 37, no. 4, pp. 849–855, 2018.

[10] W. Sui, J. Liu, and B. Gao, "A review on disaster mechanism of quicksand with a high potential energy due to mining and its prevention and control," *Journal of China Coal Society*, vol. 44, no. 8, pp. 2419–2426, 2019.

[11] W. Sui, Y. Liang, and G. Zhang, "Study status and outlook of risk evaluation on water inrush and sand inrush mechanism of excavation and mining," *Coal Science and Technology*, vol. 39, no. 11, pp. 5–9, 2011.

[12] Y. Wei-Feng, S. Wang-Hua, J. Yo-Bing, and Z. Guo-Rong, "Experimental research on the movement process of mixed water and sand flow across overburden fissures in thin bedrock induced by mining," *Journal of China Coal Society*, vol. 37, no. 1, pp. 141–146, 2012.

[13] Y. Xu, Y. Luo, J. Li, K. Li, and X. Cao, "Water and sand inrush during mining under thick unconsolidated layers and thin bedrock in the Zhaogu No. 1 Coal Mine, China," *Mine Water and the Environment*, vol. 37, no. 2, pp. 336–345, 2018.

[14] J. H. Li, Y. C. Xu, P. Jiang, Y. G. Lian, and Y. Mou, "Study on load transmission characteristics of overburden rock above coal mining face in thin bedrock of super thick unconsolidated stratum," *Coal Science and Technology*, vol. 45, no. 11, pp. 95–100, 2017.

[15] Y. K. Liang, W. H. Sui, and J. F. Qi, "Experimental investigation on chemical grouting of inclined fracture to control sand and water flow," *Tunnelling and Underground Space Technology*, vol. 83, pp. 82–90, 2019.

[16] H. L. Wang, S. J. Chen, and W. J. Guo, "Development and application of test system for water-sand inrush," *Journal of Mining & Safety Engineering*, vol. 36, no. 1, pp. 72–79, 2019.

[17] Z. Shichuan, G. Weijia, S. Wenbin, Y. Liming, and W. Hailong, "Development and application of the series of test device of coal mine water inrush behavior," *Metal Mine*, no. 2, pp. 72–79, 2017.

[18] Q. Liu and B. Liu, "Experiment study of the failure mechanism and evolution characteristics of water-sand inrush geo-hazards," *Applied Sciences*, vol. 10, no. 10, 2020.

[19] R. L. Castro, K. Basaure, S. Palma, and J. Vallejos, "Geotechnical characterization of ore related to mudrushes in block caving mining," *Journal of the Southern African Institute of Mining and Metallurgy*, vol. 117, no. 3, pp. 275–284, 2017.

[20] Z. F. Haza, I. S. H. Harahap, and L. M. Dakssa, "Experimental studies of the flow-front and drag forces exerted by subaqueous mudflow on inclined base," *Natural Hazards*, vol. 68, no. 2, pp. 587–611, 2013.

[21] V. M. Javier, K. Basaure, S. Palma, and R. L. Castro, "Methodology for evaluation of mud rush risk in block caving mining," *Journal of the Southern African Institute of Mining and Metallurgy*, vol. 117, no. 5, pp. 491–497, 2017.

[22] B. Chen, S. C. Zhang, Y. Y. Li, and J. Li, "Experimental study on water and sand inrush of mining cracks in loose layers with different clay contents," *Bulletin of engineering geology and the environment*, 2020.

[23] Q. Zhang, "Hydromechanical modeling of solid deformation and fluid flow in the transversely isotropic fissured rocks," *Computers and Geotechnics*, vol. 128, no. C, article 103812, 2020.

[24] W. Q. Zhang, Z. Y. Wang, X. X. Zhu, W. Li, B. Gao, and H. Yu, "A risk assessment of a water-sand inrush during coal mining under a loose aquifer based on a factor analysis and the fisher model," *Journal of Hydrologic Engineering*, vol. 25, no. 8, article 04020033, 2020.

[25] X. Wang, K. Shi, Q. Shi, H. Dong, and M. Chen, "A normal cloud model-based method for risk assessment of water inrush and its application in a super-long tunnel constructed by a tunnel boring machine in the arid area of northwest china," *Water*, vol. 12, no. 3, 2020.

[26] Y. Peng, L. Wu, Q. Zuo, C. Chen, and Y. Hao, "Risk assessment of water inrush in tunnel through water-rich fault based on AHP-Cloud model," *Geomatics, Natural Hazards and Risk*, vol. 11, no. 1, pp. 301–317, 2020.

[27] W. F. Yang, L. Jin, and X. Q. Zhang, "Simulation test on mixed water and sand inrush disaster induced by mining under the thin bedrock," *Journal of Loss Prevention in the Process Industries*, vol. 57, pp. 1–6, 2019.

[28] W. Yang, X. Xia, B. Pan, C. Gu, and J. Yue, "The fuzzy comprehensive evaluation of water and sand inrush risk during underground mining," *Journal of Intelligent & Fuzzy Systems*, vol. 30, no. 4, pp. 2289–2295, 2016.

[29] J. W. Bai, M. Wang, Q. S. Zhang, Z. Zhu, R. Liu, and W. Li, "Development and application of a new similar material for fluid-solid coupling model test," *Arabian Journal of Geosciences*, vol. 13, no. 18, 2020.

[30] J. J. Wang, Z. N. Shi, L. Zeng, and S. X. Qi, "The effects of different nanoadditives on the physical and mechanical

properties of similar silty mudstone materials," *Advances in Civil Engineering*, vol. 2020, Article ID 8850436, 11 pages, 2020.

[31] G. Zhang, G. Guo, Y. Lv, and Y. Gong, "Study on the strata movement rule of the ultrathick and weak cementation overburden in deep mining by similar material simulation: a case study in china," *Mathematical Problems in Engineering*, vol. 2020, Article ID 7356740, 21 pages, 2020.

[32] F. Cui, C. Jia, and X. P. Lai, "Study on deformation and energy release characteristics of overlying strata under different mining sequence in close coal seam group based on similar material simulation," *Energies*, vol. 12, no. 23, 2019.

[33] L. Y. Ke and D. P. Chen, *Bulk structure mechanics*, People's Railway Press, China, 1960.

[34] Z. H. Lu, "Analysis on arching mechanism of orifice outflow of bulk agricultural materials," *Transactions of the Chinese Society of Agricultural Engineering*, vol. 7, no. 1, pp. 78–85, 2019.

[35] M. J. Zhang, L. P. Zhang, X. P. Jiang, F. Liu, and G. Zhang, "Study on the inrushing mechanism of weak cemented quicksand layer and its forecasting," *Metal Mine*, no. 10, pp. 48–50, 2002.

[36] J. H. Qian and Z. Z. Yin, *Geotechnical Principle and Calculation*, Water Conservancy and Electric Power Press, Beijing, China, 1994.